

Inserts in a Multiple-Column Format

GARY BENSON, DEBI ERPENBECK, AND JANET HOLMES

Gary Benson
MS D417
Los Alamos, NM 87545
gsb@lanl.gov

Debi Erpenbeck
MS D418
Los Alamos, NM 87545
dje@lanl.gov

Janet Holmes
MS D417
Los Alamos, NM 87545
jah@lanl.gov

ABSTRACT

A few years ago, we approached the problem of placing inserts (or “objects”) automatically in a multiple-column format. Among the issues we encountered were enabling users to place an object wherever they desired following a textual reference (the “place-it-here” option); placing objects that spanned columns into a page while maintaining text flow in a one-pass system; and creating a text-flow pattern that followed the style of the physics journal *Physical Review*. We use a stack-like method of storing objects to create solutions to these problems.

1. Introduction

In October 1986 we became intrigued by the problems caused when inserts or objects, such as figures and equations, must be placed within a multiple-column \TeX format. Such text/figures/equations formats are common in documents we process at Los Alamos National Laboratory in our composition section. Therefore, we felt we had to find a (hopefully simple) way to solve the figure-placement (or insert-placement) problem within \TeX . The goal of our first attempts was to place inserts at the top and bottom of pages in a three-column report format.

We were able to complete the \TeX coding required to solve this first problem in about forty hours and produced the desired results. However, reports designed by various groups at Los Alamos required different insert-placement rules — frequently ones that would not permit the simple top or bottom insertion. At this point, therefore, our thoughts turned to the larger problem of placing inserts either after a textual reference or down and to the right of a reference. Because of other work assignments, we produced only design notes and sketches at first. In February 1989, however, we received a request from the editors working on a journal at Los Alamos for \TeX macros that would direct the placement of inserts according to the style of the *Physical Review* in a two-column format. This gave us the opportunity to work with insert-placement rules considerably more complex than our original problem.

2. Definition of the Problem

The *Physical Review* format requires that several basic rules be followed. These are:

1. Material must be easily included into multiple-column (in this case two-column) text.
2. The insert must always follow the textual reference to it, which means that, depending on its position within the article, it could conceivably fall at the top of a page, at the bottom, or anywhere

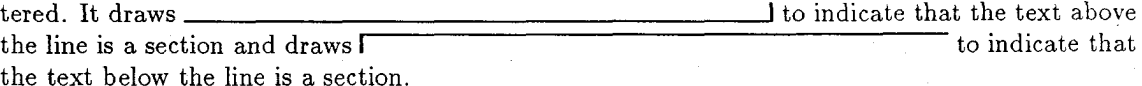
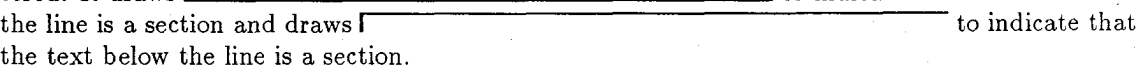
0 — the page number that is currently being processed

user specified — in which case the program will try to place the insert on the specified page

Note: this does not apply to “place-it-here”-type objects; see item 6 below.

4. `\endmulcolinsert` . Shows where the inserted object ends and places the object on the stack.
5. `\balancetothispoint` . This macro balances the material that T_EX is going to put on the current page between two columns and makes a top insert of the balanced material.
6. `\refinsertadj=a dimension value` . Use this macro to position a “place-it-here” object after its reference. We found that, in some cases, an object is not placed correctly (for example, between the word “Figure” and the number “1” with each on a separate line). This macro is a “fudge factor” to ensure proper placement in such cases, and goes before the `\beginmulcolinsert` macros.

The above macros required a few additions to format articles according to the *Physical Review* specifications. Notably, *Physical Review* uses reading flow indicators, or “reader bars,” to guide the reader’s eye in the direction of text when the text flow is interrupted by a figure or equation that spans two columns. We show an example of *Physical Review* page layout using these reader bars in Sec. 4, examples 3 and 4. The additional macros supporting a *Physical Review*-style format are given below.

1. `\phyrevtrue` . This draws reading flow indicators when a `\balancetothispoint` macro is encountered. It draws  to indicate that the text above the line is a section and draws  to indicate that the text below the line is a section.
2. `\phyrevfalse` . This cancels the effect of `\phyrevtrue` .
3. `\noclubtextlines{n}`, where *n* is the number of lines of text (“club lines”) allowed to sit by themselves in a column below an insert. At Los Alamos, we usually require five or more lines to appear in such a position, so the `\noclubtextlines` argument would be 5.
4. `\copy\upreadbarbox` . This sequence of commands creates an upward-pointing reader bar at the position specified in the text.
5. `\copy\downreadbarbox` . Likewise, this sequence of commands creates a downward-pointing reader bar at the position specified in the text.

3.4 Design and Implementation Concerns

The coding for the macros listed in Section 3.3 required about 100 hours. Up to ten objects can be stored on the stack at one time. Only versions of T_EX that have their registers doubled can process code using these macros; i.e., Sun and VAX systems.

Early in the design we realized that users may mistake features of these macros for bugs and that, to avoid user confusion, we’d better document what the code does *not* do as well as what it does do. For example, take the case of an object that is referenced in the right column but spans two columns. This situation will process correctly only if there are no multiple-column-spanning objects already in place that had been referenced in the left column. (This is a one-pass system, remember.) With this macro package, the program will place the object referenced in the right column on the next page.

We divided the processing code so that it would be easy to introduce new coding and allow fault (bug) detection. Some of the bugs we suspected were not bugs, but resulted from our inability to foresee results. There were, as usual, a number of typos and “why did I do that?”-type problems. However, there are still several elusive bugs that need to be found. For example, the following conditions occurring together in a document cause some text to be dropped:

1. The first page of the document contains a `\balancetothispoint`, which creates an object containing text and graphics that is placed on the stack as a top object. The next object is an equation.
2. The second page of the document contains two top and two bottom objects. `\noclubtextlines` is set to 5 to avoid club text at midpage.
3. The third page, like the first, contains a `\balancetothispoint`, creating an object containing text and graphics that is placed on the stack as a top object, and an equation follows as the next object. However, text is suddenly missing from the top of this page. We’ve worked around this situation by placing the two top and two bottom objects from the second page within a full-page object, but this fix seems clumsy.

4. Examples

4.1 Example 1: A Simple Example



Fig. 1. This an example of a top object that spans 2 columns

1. Introduction

The Proton Storage Ring (PSR) at Los Alamos functions as a high-current accumulator or pulse compressor to provide intense pulses of 800 MeV protons for the Los Alamos Neutron Scattering Center (LANSCE) spallation Neutron Source. The neutron scattering community has seen several proposals for similar neutron sources based on compressor rings fed from a proton linac e.g., SNQ from Jülich, one from Moscow, JHP from Japan, and (*Second Figure*)

1.1 Layout

The layout of PSR in relationship to other relevant facilities at the LAMPF site is shown schematically but not to scale in Fig. 1. An 800 MeV H⁻ beam from the LAMPF linac is kicked into Line D and transported through Line D and the Ring Injection Line to a high-field stripper magnet where it is converted with 100% efficiency to H⁺. The H⁺ beam then enters the lattice of the ring through a dipole and is stripped to H⁰ beam with ~ 92% efficiency in a 200 μg/cm² carbon foil. Up to 2800 turns

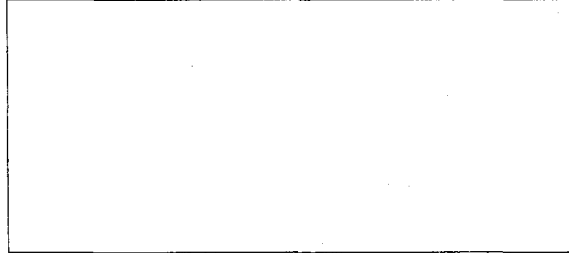


Fig. 2. This is an example of a "place it here" or referenced object

LANSCE II from Los Alamos. To date, only the PSR has been constructed, hence the experience with PSR should be helpful in assessing this approach to the design of advanced neutron sources. can be injected and accumulated during a single macropulse. Beam is normally extracted in a single turn shortly after the end of injection and transported to the LANSCE neutron production target

This is a simple example of a page with two inserted objects. The first is a top object and is placed automatically at the top of the page. The second is a "place it here" (or referenced) object that is placed about midway on the page after its reference in the text. (Note that the object is placed correctly after its reference.) The reference point is flagged by "(*Second Figure*)". The first part of the T_EX code for this example is given below.

The first object's coding was placed before the start of the text. By coding this way, a compositor can group all the top and bottom objects in a report together in one place. Compositors like this feature because they tend to think of object placement in terms of "Fig. 1 at the top of page 5, Picture 3a at bottom of page 7," etc. However, because the number of objects that can be placed on a stack at any one time is ten, a report with more than ten inserts will require more than one grouping of top and bottom objects. Only the referenced objects must be embedded within text.

```
%
%
%   ex1.tex
%
\vsiz=50pc           % Set the vsize so macros know its value
\hsiz=39pc           % Set the hsize
\input mulcol2       % Load the mulcol/inserts macros
\input ex_macros     % Load the macros for the examples
\parskip=0pt

\beginmulcol{2}{18.5pc} % Begin multiple columns
%
% First figure, a top object
%
\beginmulcolinsert{t}{2}{1}{1}
\lfigure{10pc}{30pc}{This an example of a top object that spans 2
columns}{ }
\endmulcolinsert

\leftline{\bf I. INTRODUCTION}
The Proton Storage Ring (PSR) at Los Alamos functions as a high-current
accumulator or pulse compressor to provide intense pulses of 800 MeV
protons for the Los Alamos Neutron Scattering Center (LANSCE) spallation
Neutron Source. The neutron scattering community has seen several
proposals for similar neutron sources based on compressor rings feed from a
proton linac e.g., SNQ from Jülich, one from Moscow, JHP from Japan, and
(*Second Figure*)
```

A portion of the log for example 2

```
The insert starts in the left column
and only spans the left column
>> Placing bottom insert number 4
The insert starts in the right column
and spans only the right column
>> Removing insert 3, from stack
>> Removing insert 4, from stack
>> [Finished page 2]
[3]
>> Processing insert number 9, to be placed on page 3
>> Processing insert number 10, to be placed on page 3
>> Processing insert number 11, to be placed on page 3
>> Processing insert number 12, to be placed on page 4
>> Processing insert number 13, to be placed on page 4
>> Processing insert number 14, to be placed on page 4
>> Insert 9, and reference moving to page 4
>> Insert 10, and reference moving to page 4
>> Insert 11, and reference moving to page 4
>> Insert 8, referenced in left column
and spans the right column
>> Placing referenced insert number 8

Overfull \vbox (0.38889pt too high) has occurred while \output is active
>> Removing insert 8, from stack
>> [Finished page 3]
[4]
>> Insert 11, will not fit in left column
Moving it to page 5, as a top insert and
leaving the reference on the current page
>> Placing top insert number 7
The insert starts in the right column
and spans only the right column
>> Placing top insert number 6
The insert starts in the left column
and only spans the left column
>> Placing top insert number 5
The insert starts in the left column
and spans the right column
>> Placing bottom insert number 12
The insert starts in the left column
and only spans the left column
>> Placing bottom insert number 13
The insert starts in the right column
and spans only the right column
>> Placing bottom insert number 14
The insert starts in the left column
>> Insert 9, referenced in left column
and spans the right column
>> Placing referenced insert number 9
```

4.3 Example 3: What's Nice About the Fizzrev Shuffle.

This example illustrates the use of the macros to produce *Physical Review*-style documents and illustrates the advantage of using this style.

The example is broken up into two sections. The first section represents the output without using the *Physical Review* style; the second section shows the result of using this style. The example makes up a "before-and-after" sequence.

Before

5.1.8 Determination of Peak Position by a Linearized Gaussian Fit

This procedure transforms the Gaussian shaped peak into a line and then fits a line to the transformed peak. The slope and intercept of the fitted line are related to a_0 and σ . The background continuum under the peak is first subtracted so that

$$s^2 y(x) = y(x) - \frac{1}{4} \left[k^2 \frac{(x-x_0)^2}{N^2} - (2-k) \frac{y_0}{N^2} \right] \quad (5-17)$$

where

$$k = \frac{y(x-x_0)}{(x_1-x_0)}$$

the fit is made only to the Gaussian-shaped peak.

Transformations that linearize the Gaussian function have been applied only recently to determine the parameters of gamma-ray peaks (Ref. 7). The simplest of a class of similar transformations is the function

$$Q(x) = \ln \frac{y(x-1)}{y(x-1)} = \frac{2}{\sigma^2} x - \frac{2x_0}{\sigma^2} \quad (5-18)$$

where $y(x)$ is the number of counts in channel x . The last expression in Equation 5-18 is correct if $y(x)$ is the usual Gaussian function. The linear function $Q(x)$ has a slope m and intercept b given by

$$m = 2/\sigma^2$$

$$b = -2x_0/\sigma^2 \quad (5-12)$$

Solving for σ^2 and a_0 gives

$$\sigma^2 = 2/m$$

$$a_0 = -b/m \quad (5-13)$$

Equation 5-14 gives the expressions for the slope m and the intercept b of the line fit to the set of points $\{x_i, Q(x_i)\}$ by the weighted-least-squares method: (*5-14*)

$$s^2 Q(x_i) = s^2 y(x_i - 1) - s^2 y(x_i - 1) \quad (5-15)$$

$$m = \frac{1}{\Delta} \left(\sum \frac{x_i}{\sigma_i^2} \sum \frac{Q_i}{\sigma_i^2} - \sum \frac{Q_i}{\sigma_i^2} \sum \frac{x_i}{\sigma_i^2} \right)$$

where $\sigma_i = \sigma(x_i)/y_i$.

If the background continuum is small enough to ignore, then the variance becomes

Eq. 5.3.3.

For a linear fit there are simple expressions for the estimated variance s^2 of m and b .

$$s^2(m) = \frac{1}{\Delta} \sum \frac{1}{\sigma_i^2}$$

$$s^2(b) = \frac{1}{\Delta} \sum \frac{x_i^2}{\sigma_i^2} \quad (5-16)$$

Although the fitting procedure just described may seem somewhat complex, the fit can be performed by a short computer program in only a few seconds. The Gaussian function should be fit to the top three-fourths to two-thirds of the peak to avoid problems with non-Gaussian tails and imprecise data. The x channels in the peak give $n-2$ values of $Q(x)$. When at least four or five values of $Q(x)$ are used in the fit, the results are more than adequate to determine the peak centroid needed for the energy calibration. Unfortunately, it is very difficult to estimate the statistical uncertainty in a_0 using the fitting procedure. However, experience indicates that for peaks of reasonable precision, the values of a_0 are good to ~ 0.1 channel or better.

In automated operations, a test should be made to determine whether a Gaussian function adequately describes the input data. The reduced chi-square statistic χ^2/ν provides such a test. For the linear fit of $Q(x)$ versus x , (*5-19*) where n and b are computed from Equation 5-14 and m is the number of values of $Q(x)$ in the fit. For good fits, χ^2/ν should be ~ 1.00 . (See Ref. 5 for a very readable discussion of the properties of χ^2/ν .) For low-precision peaks (up to ~ 10 000 counts/channel), χ^2/ν is really ~ 1.00 for peaks of

$$b = \frac{1}{\Delta} \left(\sum \frac{x_i^2}{\sigma_i^2} \sum \frac{Q_i}{\sigma_i^2} - \sum \frac{x_i}{\sigma_i^2} \sum \frac{Q_i}{\sigma_i^2} \right) \quad (5-14)$$

$$m = \frac{1}{\Delta} \left(\sum \frac{1}{\sigma_i^2} \sum \frac{x_i Q_i}{\sigma_i^2} - \sum \frac{x_i}{\sigma_i^2} \sum \frac{Q_i}{\sigma_i^2} \right)$$

where

$$\Delta = \sum \frac{1}{\sigma_i^2} \sum \frac{x_i^2}{\sigma_i^2} - \left(\sum \frac{x_i}{\sigma_i^2} \right)^2$$

$s^2 =$ estimated variance of $Q(x)$.

$$\chi^2/\nu = \frac{1}{n-2} \left\{ \sum \frac{1}{\sigma_i^2} \left[Q_i - (mx_i + b) \right]^2 \right\} \quad (5-19)$$

qualitatively good shape. As the maximum number of counts per channel increases, χ^2/ν increases even though the peak shape remains the same. The increase in χ^2/ν does not necessarily mean the fit is inadequate for determining energy calibrations or for testing resolution. At low precision, the goodness of fit is dominated by counting statistics; at high precision it is dominated by the inevitable small deviations of the peak shape from a true Gaussian shape, resulting in an increase in the computed value of χ^2/ν . Experience will dictate an acceptable value of χ^2/ν for a given range of peak precision.

Figure 5.6 shows a low-precision spectral peak from a germanium detector (FWHM $\sim 1\%$ channels) with the fitted Gaussian function superimposed upon it. The lower portion of the figure shows the plot of $Q(x)$ versus x for the upper two-thirds of the peak along with the fitted line and the computed peak parameters.

5.1.9 Determination of Peak Position Using a Parabolized Gaussian Fit

The natural logarithm of the Gaussian function is parabolic, as is strikingly apparent when full-energy peaks are viewed using the logarithmic display of an MCA. The natural logarithm of the Gaussian (Equation 5-6) gives

$$\ln y = c_2 x^2 - c_1 x - c_0 \quad (5-20)$$

$$c_2 = -1/2\sigma^2$$

$$c_1 = x_0/\sigma^2$$

$$c_0 = \ln y_0 - x_0^2/2\sigma^2$$

A fit of Equation 5-20 to the set of points $\{x_i, \ln y_i\}$ produces values of c_2 , c_1 , and c_0 that give the parameters of the Gaussian:

$$x_0 = -c_1/2c_2$$

$$\sigma = \sqrt{-1/2c_2}$$

$$\ln y_0 = c_0 - c_1^2/4c_2 \quad (5-21)$$

The fitted curve is a parabola that opens downward and whose axis is parallel to the x -axis. The procedure described here determines y_0 in addition to a_0 and σ , the two parameters obtained from the linear fit to the linearized Gaussian. Therefore, the full-energy peak area can be determined using Equation 5-8.

Figure 5.7 shows a parabolized Gaussian fit to a high-precision spectral peak from the 122.0-keV gamma-ray of ^{56}Co . The same high-quality germanium detector was used in this figure as in Figure 5.6(a). At low energies, charge collection in germanium detectors is more complete than at high energies, with a resultant decrease in low-energy tailing. Comparison of Figure 5.6(a) and 5.7 shows that the tailing in the 122-keV peak of Figure 5.7 is even less than the small tailing of the 1332-keV

The points of reference of the objects (equations) being inserted are flagged with "(* eq. no. *)" — for example, (*5-14*).

On the first page of the "before" example, the equations flow correctly up until Eq. 5-14. This equation did not appear after its reference because of its size; thus, it was moved to the top of the next page. Equation 5-17 is referenced in the right column and placed two lines below its reference. This could have been corrected by use of the `\refinsertadj` dimension register. Equation 5-19 was too large to fit after its reference and thus was moved to the top of the next page.

The only two-column-spanning equations that were set correctly in the "before" example are Eqs. 5-22 and 5-24, which occur on page 3.

peak in Figure 5.6(a).

The expressions for the weighted quadratic least-squares fit are included for the convenience of possible users. The expressions are given in determinant form and involve eight sums, indicated by S1, S2, ..., S8. (*5-22*)

$$c_0 = \frac{1}{\Delta} \begin{vmatrix} S6 & S2 & S3 \\ S7 & S3 & S4 \\ S8 & S4 & S5 \end{vmatrix}$$

$$c_1 = \frac{1}{\Delta} \begin{vmatrix} S1 & S6 & S3 \\ S2 & S7 & S4 \\ S3 & S8 & S5 \end{vmatrix} \quad (5-22)$$

$$c_2 = \frac{1}{\Delta} \begin{vmatrix} S1 & S2 & S6 \\ S2 & S3 & S7 \\ S3 & S4 & S8 \end{vmatrix}$$

where

$$\Delta = \begin{vmatrix} S1 & S2 & S3 \\ S2 & S3 & S4 \\ S3 & S4 & S5 \end{vmatrix}$$

$$S1 = \sum \frac{1}{\sigma_i^2} \quad S2 = \sum \frac{x_i}{\sigma_i^2} \quad S3 = \sum \frac{x_i^2}{\sigma_i^2} \quad S4 = \sum \frac{y_i}{\sigma_i^2}$$

$$S5 = \sum \frac{x_i y_i}{\sigma_i^2} \quad S6 = \sum \frac{\ln y_i}{\sigma_i^2} \quad S7 = \sum \frac{x_i \ln y_i}{\sigma_i^2} \quad S8 = \sum \frac{x_i^2 \ln y_i}{\sigma_i^2}$$

As usual, the sums are over all the points fit. The y_i values have the background continuum subtracted. The remaining expressions required for the fitting procedure are

$$a_i = s(\ln y_i)$$

$$s(\ln y) = \frac{s(y)}{y \ln y} \quad (5-23)$$

where $s(y)$ is given by Equation 5-17. The expression for χ^2/ν , the goodness-of-fit statistic, is (*5-24*)

$$\chi^2/\nu = \frac{1}{n-3} \left\{ \sum \frac{1}{\sigma_i^2} \left[\ln y_i - (c_2 x_i^2 - c_1 x_i - c_0) \right]^2 \right\} \quad (5-24)$$

where n is the number of points fit and c_2 , c_1 , and c_0 are the values computed from Equation 5-22.

The remarks made in the previous section about the portion of the peak to be fit and about trends in χ^2/ν values apply equally well here. The quadratic fits put considerable demands on the computer, and occasionally the six significant decimal digits provided by many 16-bit processors run

5.1.10 Determination of Peak Position Using Complex Spectral Fitting Codes

Large fitting codes are used to analyze complex spectra with overlapping peaks. The codes describe the peaks with functions that have a basic Gaussian form, with tailing functions added to describe the peak shape more accurately. An iterative nonlinear least-squares procedure is used to fit the data. The centroid of the Gaussian component of the fitted

peak is taken as the peak position for purposes of energy determination.

```

% material in TeX's memory
\beginmulcolinsert{r}{2}{1}{pg.no.} % r=right here, 2=spans two columns,
1=starts
% in 1st column, pg.no.=on this page #
the object % Equation, figure, table, text, or
combination
\endmulcolinsert % End of the object and single column mode

```

In addition to the objects discussed above, the fizzle macro package formats a journal's title page, figure captions (including figures inserted with the psfig macro package), three levels of section headings, and textual references and numbers for equations (using a placeholder instead of an equation number). The line lengths of the title and running heads are both user-adjustable. See the listing below for definitions of available macros in the fizzle package.

Using the two-column macros from inside one's own macros makes writing macros like `\refrule` easier; neither the macro designer nor the user needs to worry about the details of getting out of two-column mode to center the rule. The following coding was required to implement the reference rule:

```

\def\refrule{ % Begin def
  \phyrevfalse % Don't draw reading flow indicators here
  \beginmulcolinsert{r}{2}{1}{0} % r=the rule is an insert, 2=spanning
  % two columns, 1=starting in the
  % left column, 0=on current page
  \vskip2pc % Leave some white space
  \centerline{\vrule width16.5pc depth0pt height.5pt} % Center the line
  \vskip1.5pc % Leave more white space
  \endmulcolinsert % End of insert
  \phyrevtrue % Set indicators back on
}

```

4.5 Fizzle Macro Definitions

Following each definition, is an example of how to use the macro in a paper. See the Fizzle Users Guide for complete descriptions.¹

```

\abstract{}: formats the abstract. The argument is the text of the abstract.
\abstract{This is an abstract.}

\affil{}: for the name of the author's affiliation. The argument is the
name of the affiliation.
\affil{Los Alamos National Laboratory}

\authors{}: used when there is more than one author/affiliation pair.
\authors{Jane Doe}\affil{Sandia National Laboratory}

\autoauthorfalse or true: switch for user control of running author headline. It is set true
in the fizzle package to enable automatic generation of a run-
ning author headline on even-numbered pages. \autoauthor-
false will cause the macros to prompt the user for a running
author headline.

\autotitlefalse or true: switch for user control of running title headline. It is set true in
the fizzle package to enable automatic generation of a running
title headline on odd-numbered pages. \autotitlefalse will
cause the macros to prompt the user for a running title headline.

```

¹ Available from the authors.

<code>\beginmc{}</code> :	abbreviation for the multi-column <code>\beginmulcol</code> macro. <code>\beginmc{2}{20.5pc}</code>
<code>\binsert{}{}{}{}:</code>	abbreviation for the multi-column <code>\beginmulcolinsert</code> macro. <code>\binsert{r}{2}{1}{2}</code> "Place it right here, span 2 columns, start in 1st column, and put the object on page 2."
<code>\bttp:</code>	abbreviation for the multi-column <code>\balancetothispoint</code> macro.
<code>\einsert:</code>	abbreviation for the multi-column <code>\endmulcolinsert</code> macro.
<code>\endmc:</code>	abbreviation for the multi-column <code>\endmulcol</code> macro.
<code>\eq:</code>	used to reference an equation in the text and number it. "See Equation <code>\eq{\qa}</code> . $A + B = C$ <code>\eqno{\qa}</code> ." <code>\qa</code> is just a placeholder, the <code>\eq</code> macro will evaluate the placeholder to the current number stored in the equation counter.
<code>\fig{}{}{}{}:</code>	used to set the caption and leave space for the figure. Argument 1 is the height of the figure, argument 2 is the width of the figure, argument 3 is the caption excluding a label (i.e., Fig. 1), and argument 4 is a switch for a box outline (set to 1 for on, 0 for off). <code>\fig{20pc}{20.5pc}{This is a caption.}{1}</code>
<code>\figcount:</code>	used to control the figure number. <code>\figcount=3</code> to get a figure labelled "Fig. 4".
<code>\getheaderfooterinfo{}{}{}{}:</code>	provides the information for the header and the footer. Argument 1 is the volume number, argument 2 is the issue number, argument 3 is the title, and argument 4 is the author's name. <code>\getheaderfooterinfo{12}{35}{Title}{Author}</code>
<code>\it:</code>	used for standard italics text. <code>\it{emphasis}</code>
<code>\jtp:</code>	used to set a journal titlepage and page parameters. See also <code>\ptp</code> .
<code>\letter{}</code> :	used for figures that are lettered, i.e., Fig. 1A. The argument is the needed letter. <code>\letter{A}</code>
<code>\ninepoint:</code>	for text and math at nine point. Shouldn't be needed but it is available. <code>{\ninepoint This text will be in 9-point.}</code>
<code>\page{}</code> :	used instead of <code>\pageno</code> macro. The argument is the first page of the journal or the paper. <code>\page{1}</code>
<code>\phyrevfalse</code> or <code>true:</code>	switch that controls the drawing of reading flow indicators, true for on, false for off. Set to true in the fizzle package.
<code>\postscriptfig{}{}{}:</code>	for use with PSFIG macro package. Argument 1 is the height of the figure, argument 2 is the width of the figure, argument 3 is the figure caption, excluding a label (i.e., Fig. 1), and argument 4 is the name of the PostScript file. <code>\postscriptfig{20pc}{20.5pc}{This is a caption.}{figure1.ps}</code>
<code>\ptp:</code>	for a paper's title page. Will set up the <code>\vsize</code> and the headline size for a paper.
<code>\recvd{}</code> :	argument is a date. The word "Received" and the opening and closing parentheses are added by the macros and centered. <code>\recvd{3 March 1989}</code>

mode-coupling theory, as developed by Ernst *et al.*,^{13, 15, 17} and considered the multicomponent and double-particle systems in addition to the plane hydrodynamics of Pomeau. Because the form of the mode-coupling results depends on the form of the starting hydrodynamic equations, it is evident that the long-time tails for a given set of time-correlation functions will have different forms when expressed in terms of the different set of transport coefficients.

Wood²² considered the case of a binary mixture in *d* dimensions, assuming that the equation of state and transport coefficients are known. In addition to calculating, except for numerical approval simplices, the results of Pomeau²² for the long-time tails in the plane system of fluxes and forces, he also obtained relatively simple expressions for the tails for the double-particle system and somewhat more complicated expressions for the momentum systems. In this section we display the mode-coupling results for the latter.

The general form of the long-time tail for transport coefficient *L_i* is

$$L_i(t) \sim k_i t^{-d/2} \quad (10)$$

It is perhaps simplest to write the coefficient *L_i* in terms of the double-particle transport coefficients rather than the mainstream coefficients. For thermal diffusion, then, the coefficient *L₁* is

$$k_{11} = \frac{d}{d^2 \mu_1 \eta_1} \sum_{\alpha, \beta} \frac{\eta_{\alpha\beta}}{4\pi(\eta_1 + \eta_2)} \frac{L_{\alpha\beta}^* L_{\alpha\beta}^*}{\eta_1 \eta_2} \quad (11)$$

in which

$$\eta_{\alpha\beta} = \frac{1}{2} (\mu_{\alpha\beta} L_{\alpha\beta}^* + L_{\alpha\beta}^* \mu_{\alpha\beta} / \eta_1 \eta_2), \quad (12)$$

$$\mu_{\alpha\beta} = \left(\frac{\partial \mu}{\partial c_1} \right)_{T, p} \quad (13)$$

and in which *c₁* is the specific constant-pressure heat capacity. For thermal diffusion, the coefficient is

$$k_{11} = \frac{d}{d^2 \mu_1 \eta_1} \sum_{\alpha, \beta} \frac{\eta_{\alpha\beta}}{4\pi(\eta_1 + \eta_2)} \frac{L_{\alpha\beta}^* L_{\alpha\beta}^*}{\eta_1 \eta_2} \quad (14)$$

For thermal conductivity, the long-time tail coefficient is

$$k_{11} = \frac{d}{d^2 \mu_1 \eta_1} \sum_{\alpha, \beta} \frac{\eta_{\alpha\beta}}{4\pi(\eta_1 + \eta_2)} \frac{L_{\alpha\beta}^* L_{\alpha\beta}^*}{\eta_1 \eta_2} \quad (15)$$

By virtue of Eq.(2) relating the double-particle transport coefficients to the mainstream coefficients, we regard these expressions as providing the mainstream long-time tails in terms of the mainstream transport coefficients.

III. MONTE CARLO, MOLECULAR DYNAMICS CALCULATIONS

In this section, we discuss the evaluation of the transport coefficients directly from the Green-Kubo formulas for a 511-511 binary mixture of hard spheres (*d* = 3), of species having diameter σ , or, for the particular species having a mass of 0.101. Because the thermodynamic and transport variables have a trivial dependence on temperature for hard spheres, we specify the state through the volume relative to *N*. We have used the highest "Ranking approximation" (*i.e.*, highest degree B-spline polynomial expansion) for which the

in which *v* is the adiabatic sound speed,

$$v^2 = \left(\frac{\partial p}{\partial \rho} \right)_{T, n_1} \quad (16)$$

and *v₁* is the acoustic damping constant,

$$v_1 = \frac{1}{\rho} \left[\frac{\partial \rho}{\partial \rho} \right]_{T, n_1} \quad (17)$$

in which

$$X = \frac{\rho}{\rho_0} \left(\frac{\partial \rho}{\partial \rho} \right)_{T, n_1} \quad (18)$$

is related to the usual volume coefficient of thermal expansion and

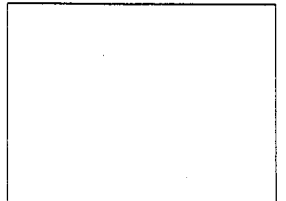
$$\mu_p = \left(\frac{\partial \mu}{\partial p} \right)_{T, n_1} \quad (19)$$


FIG. 1. Time-dependent thermal conductivity, relative to the Rankin value, for a 511-511 binary hard-sphere mixture having mass ratio of 0.1 and diameter ratio of 1.0 at a volume of time times close packing, as a function of the time *t*, relative to the observed mean free time *t₀* for a 511-particle system. The curve shows the moments we have derived for the system. The error bars represent ±1 standard deviation from the mean.

IV. CONCLUSIONS

We list here what seem to be the most important conclusions that can be drawn from this work.

1. The transport coefficients for mixtures can be defined in a variety of ways by virtue of the fact that the separation of the heat current into a thermal and a diffusive part is not unique, even when subject to the Onsager conditions. From the point of view of molecular dynamics calculations, the mainstream choice of fluxes and forces, with driving forces of $\nabla^2 T$ and $\nabla^2 (\mu_1 / T)$, yields Green-Kubo expressions which do not require knowledge of the partial specific enthalpies for the system and are, therefore, more easily applied.
2. For the mass and diameter ratio obtained here at a volume of 1 times close-packing, the long-time behavior of the time-correlation functions for shear viscosity, thermal conductivity, thermal diffusion, and mutual diffusion appear to agree (within their statistical uncertainties) with the predictions of the mode-coupling theory. Except for the strong evidence for agreement in the case of one-component self-diffusion,^{15, 17} the present evidence seems to be the first to support mode-coupling theory for other time-correlation functions. Whether this agreement holds for other densities and for other mass and diameter ratios remains to be seen.
3. The results for the hard-sphere transport coefficients agree (within their statistical uncertainties) with the predictions for the isotropic mixture above significant deviations from the Rankin theory. These deviations arise principally from the

long-time tails of the time correlation functions, as can be seen from Table II. The values of *L_i*(35*t₀*) show quite modest deviations from unity, even though the time is long compared to the Rankin decay time. The additional contributions for longer times are small for shear viscosity, but increasingly large for mutual diffusion (75%), thermal diffusion (115%), and thermal conductivity (10%). This result contrasts with the conclusion of Alder and Wainwright¹⁰ for the thermal conductivity of a single-component, hard-sphere fluid but agrees with their observations for shear viscosity.

4. The present results suggest that further study of the parameter space for hard-sphere mixtures is in order. Calculations for other densities and for a number of other mass and diameter ratios are now in progress.

ACKNOWLEDGMENT

The author is grateful to W. W. Wood of Cornell College for extensive discussions of the mixture problem and for making his results for the long-time tails available before publication. He is also grateful to J. M. Kincaid of the State University of New York at Stony Brook, E. G. D. Cohen

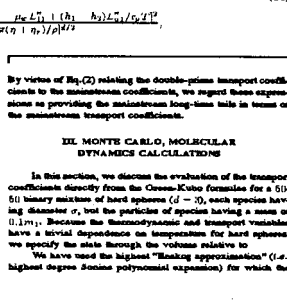


FIG. 2. Reduced transport coefficients for a 511-511 binary hard-sphere mixture having mass ratio of 0.1 and diameter ratio of 1.0, evaluated at a time *t₀* of approximately 1100 mean free times, as a function of the component of the total number of particles *N_i*, showing the dependence on system size. The various transport coefficients are $\alpha = \mu$ for thermal conductivity, β for thermal diffusion, γ for mutual diffusion, and η for shear viscosity. The lines are a smoothed least-squares fit for each set of data. The standard deviation error bars (± 1 standard deviation) are not shown for all of the *N_i* = 4110 data; see Table I for the values.

of Rockefeller University, and M. Lopez de Haro of Instituto de Investigaciones en Matematicas, Universidad Nacional Autonoma de Mexico for numerous discussions and for providing the evaluation of the Rankin transport coefficients and their help in modifying these programs to yield the desired form of the coefficients.

This work was supported by a contract with the U. S. Department of Energy, Office of Basic Energy Sciences, Division of Chemical Sciences.

1. D. E. Hering, *Svezhita Vozmozhnost*, *Izv.* 63, 4 (1952).
2. S. Chapman and T. G. Cowling, *The Mathematical Theory of Nonuniform Gases*, Cambridge University Press, Cambridge, 1939, Second edition.
3. H. van Beijeren and M. H. Ernst, *Physica* 68, 437 (1973).
4. H. van Beijeren and M. H. Ernst, *Physica* 70, 225 (1973).
5. M. K. Than and K. E. O'Connell, *J. Chem. Phys.* 65, 268 (1971).
6. M. Lopez de Haro, E. G. D. Cohen, and J. M. Kincaid, *J. Chem. Phys.* 78, 3746 (1983).
7. J. M. Kincaid, M. Lopez de Haro, and E. G. D. Cohen, *J. Chem. Phys.* 79, 4509 (1983).
8. J. M. Kincaid, E. G. D. Cohen, and M. Lopez de Haro, *J. Chem. Phys.* 80, 937 (1987).
9. B. J. Alder and T. E. Wainwright, *Phys. Rev. Lett.* 16, 988 (1967).
10. B. J. Alder and T. E. Wainwright, *Phys. Rev. A* 1, 18 (1970).
11. J. J. Eppenberg and W. W. Wood, *Phys. Rev. A* 20, 1648 (1982).
12. J. J. Eppenberg and W. W. Wood, *Phys. Rev. A* 33, 412 (1985).
13. J. R. Dorfman and E. G. D. Cohen, *Phys. Rev. A* 6, 776 (1972).
14. E. R. Dorfman and E. G. D. Cohen, *Phys. Rev. A* 12, 292 (1975).
15. M. H. Ernst, B. H. Hoge, and J. M. J. van Leeuwen, *Phys. Rev. A* 4, 2035 (1971).
16. M. H. Ernst, B. H. Hoge, and J. M. J. van Leeuwen, *J. Stat. Phys.* 10, 7 (1976).
17. M. H. Ernst, B. H. Hoge, and J. M. J. van Leeuwen, *J. Stat. Phys.* 10, 23 (1976).
18. B. J. Alder, D. M. Chen, and T. E. Wainwright, *J. Chem. Phys.* 53, 3813 (1970).
19. T. R. Kirkpatrick, *Phys. Rev. Lett.* 53, 1733 (1984).
20. I. M. de Schipper, A. F. Hoogmoed, and H. van Beijeren, *Phys. Rev. Lett.* 57, 1715 (1986).
21. G. Jacucci and I. R. McDonald, *Physica* A 60, 607 (1972).
22. C. Hohenberg and U. Dunsm, *ibid.* *Phys.* 37, 95 (1979).
23. A. A. Chiford and R. Dickason, *Mol. Phys.* 34, 873 (1977).
24. D. L. Jolly and R. J. Burman, *Mol. Phys.* 41, 137 (1980).
25. M. Schoone and C. Hohenberg, *Mol. Phys.* 52, 95 (1984).
26. M. Schoone and C. Hohenberg, *Mol. Phys.* 55, 1029 (1984).
27. R. Vögelsang and C. Hohenberg, *Phys. Rev. A* 35, 3487 (1987).
28. D. MacGowan and D. J. Evans, *Phys. Rev. A* 34, 2155 (1986).
29. S. R. de Groot, *Thermodynamics of Irreversible Processes*, North-Holland, Amsterdam, 1951.
30. W. W. Wood, *Mode-Coupling Theory for the Long-Time Tails for the Transport Coefficients of Mixtures*, (in preparation).
31. S. R. de Groot and P. Mazur, *Nonequilibrium Thermodynamics*, North-Holland, Amsterdam, 1962.
32. H. J. Green, *J. Math. Phys.* 2, 344 (1961).
33. Y. Pomeau, *J. Chem. Phys.* 57, 2300 (1972).
34. J. J. Eppenberg and W. W. Wood, *J. Stat. Phys.* 24, 455 (1981).
35. J. M. Kincaid, (private communication).
36. J. M. Kincaid and J. J. Eppenberg, *The Mutual Diffusion Constant of Binary Isotropic Hard-Sphere Mixtures: Molecular Dynamics Calculations using the Green-Kubo and Steady State Methods*, 1986.

FORTRAN package was designed, namely the least approximation.

In similar fashion, we determine the long-time tails of the time-correlation functions from these double-particle transport coefficients, obtaining the required thermodynamic quantities. For example, to obtain μ_p we use

$$\left(\frac{\partial \mu}{\partial c_1} \right)_{T, p} = \sum_{\alpha, \beta} \left(\frac{\partial \mu}{\partial n_{\alpha\beta}} \right)_{T, n_1, n_2} \left(\frac{\partial n_{\alpha\beta}}{\partial c_1} \right)_{T, p} \quad (20)$$

$$\left(\frac{\partial n_{\alpha\beta}}{\partial c_1} \right)_{T, p} = \frac{1}{J_2} \left(\frac{\partial p}{\partial n_{\alpha\beta}} \right)_{T, n_1, n_2} \quad (21)$$

$$\left(\frac{\partial p}{\partial n_{\alpha\beta}} \right)_{T, n_1, n_2} = \frac{m_{\alpha\beta} m_{\gamma\delta}}{(m_{\alpha\beta} + m_{\gamma\delta})^2} \sum_{\gamma, \delta} \left(\frac{\partial p}{\partial n_{\gamma\delta}} \right)_{T, n_1, n_2} \quad (22)$$

which can be readily evaluated.

A. Numerical Results

Our calculations include the study of systems of 1100, 510, 1372, and 4110 particles. The parameters for each of these calculations are given in Table I, including the time steps per trajectory *N_t*, and the number of trajectories *N_t*. Observe that for the larger systems the trajectories are relatively short on the basis of the number of collisions per particle. Because the number of trajectories for the larger systems is not proportionately larger, the calculations for the larger systems, especially the 4110-particle system, are relatively less extensive when applied to the calculation of fluctuation functions for the transport properties studied here.

Our results concern the time-dependent transport coefficients, either evaluated directly from, as in the case of mutual diffusion and thermal diffusion, or through differentiations of the Einstein function, as in the case of the thermal conductivity and the viscosity. We define reduced transport coefficients relative to the Rankin values (in the least squares approximation) by adding a caret over the symbol, *e.g.*,

$$\hat{L}_i = L_i / L_i^R \quad (23)$$

The Rankin transport coefficients are evaluated as outlined above, yielding

$$\hat{L}_1^R = 3.0107430 \frac{m_1}{(m_1 + m_2)^2 \eta_1^2} \quad (24)$$

$$\hat{L}_2^R = 0.0540929 \frac{m_1}{(m_1 + m_2)^2 \eta_1^2} \quad (25)$$

$$\hat{L}_3^R = 0.0021144 \frac{m_1}{(m_1 + m_2)^2 \eta_1^2} \quad (26)$$

$$\hat{L}_4^R = 0.2937602 \frac{m_1}{(m_1 + m_2)^2 \eta_1^2} \quad (27)$$

of Rockefeller University, and M. Lopez de Haro of Instituto de Investigaciones en Matematicas, Universidad Nacional Autonoma de Mexico for numerous discussions and for providing the evaluation of the Rankin transport coefficients and their help in modifying these programs to yield the desired form of the coefficients.

This work was supported by a contract with the U. S. Department of Energy, Office of Basic Energy Sciences, Division of Chemical Sciences.

1. D. E. Hering, *Svezhita Vozmozhnost*, *Izv.* 63, 4 (1952).
2. S. Chapman and T. G. Cowling, *The Mathematical Theory of Nonuniform Gases*, Cambridge University Press, Cambridge, 1939, Second edition.
3. H. van Beijeren and M. H. Ernst, *Physica* 68, 437 (1973).
4. H. van Beijeren and M. H. Ernst, *Physica* 70, 225 (1973).
5. M. K. Than and K. E. O'Connell, *J. Chem. Phys.* 65, 268 (1971).
6. M. Lopez de Haro, E. G. D. Cohen, and J. M. Kincaid, *J. Chem. Phys.* 78, 3746 (1983).
7. J. M. Kincaid, M. Lopez de Haro, and E. G. D. Cohen, *J. Chem. Phys.* 79, 4509 (1983).
8. J. M. Kincaid, E. G. D. Cohen, and M. Lopez de Haro, *J. Chem. Phys.* 80, 937 (1987).
9. B. J. Alder and T. E. Wainwright, *Phys. Rev. Lett.* 16, 988 (1967).
10. B. J. Alder and T. E. Wainwright, *Phys. Rev. A* 1, 18 (1970).
11. J. J. Eppenberg and W. W. Wood, *Phys. Rev. A* 20, 1648 (1982).
12. J. J. Eppenberg and W. W. Wood, *Phys. Rev. A* 33, 412 (1985).
13. J. R. Dorfman and E. G. D. Cohen, *Phys. Rev. A* 6, 776 (1972).
14. E. R. Dorfman and E. G. D. Cohen, *Phys. Rev. A* 12, 292 (1975).
15. M. H. Ernst, B. H. Hoge, and J. M. J. van Leeuwen, *Phys. Rev. A* 4, 2035 (1971).
16. M. H. Ernst, B. H. Hoge, and J. M. J. van Leeuwen, *J. Stat. Phys.* 10, 7 (1976).
17. M. H. Ernst, B. H. Hoge, and J. M. J. van Leeuwen, *J. Stat. Phys.* 10, 23 (1976).
18. B. J. Alder, D. M. Chen, and T. E. Wainwright, *J. Chem. Phys.* 53, 3813 (1970).
19. T. R. Kirkpatrick, *Phys. Rev. Lett.* 53, 1733 (1984).
20. I. M. de Schipper, A. F. Hoogmoed, and H. van Beijeren, *Phys. Rev. Lett.* 57, 1715 (1986).
21. G. Jacucci and I. R. McDonald, *Physica* A 60, 607 (1972).
22. C. Hohenberg and U. Dunsm, *ibid.* *Phys.* 37, 95 (1979).
23. A. A. Chiford and R. Dickason, *Mol. Phys.* 34, 873 (1977).
24. D. L. Jolly and R. J. Burman, *Mol. Phys.* 41, 137 (1980).
25. M. Schoone and C. Hohenberg, *Mol. Phys.* 52, 95 (1984).
26. M. Schoone and C. Hohenberg, *Mol. Phys.* 55, 1029 (1984).
27. R. Vögelsang and C. Hohenberg, *Phys. Rev. A* 35, 3487 (1987).
28. D. MacGowan and D. J. Evans, *Phys. Rev. A* 34, 2155 (1986).
29. S. R. de Groot, *Thermodynamics of Irreversible Processes*, North-Holland, Amsterdam, 1951.
30. W. W. Wood, *Mode-Coupling Theory for the Long-Time Tails for the Transport Coefficients of Mixtures*, (in preparation).
31. S. R. de Groot and P. Mazur, *Nonequilibrium Thermodynamics*, North-Holland, Amsterdam, 1962.
32. H. J. Green, *J. Math. Phys.* 2, 344 (1961).
33. Y. Pomeau, *J. Chem. Phys.* 57, 2300 (1972).
34. J. J. Eppenberg and W. W. Wood, *J. Stat. Phys.* 24, 455 (1981).
35. J. M. Kincaid, (private communication).
36. J. M. Kincaid and J. J. Eppenberg, *The Mutual Diffusion Constant of Binary Isotropic Hard-Sphere Mixtures: Molecular Dynamics Calculations using the Green-Kubo and Steady State Methods*, 1986.

5. What Next?

1. We need to simplify the \TeX code for these macros and make it smaller. It would be nice if PCs and Macintoshes could use it.
2. We want to start processing flowing text as objects.
3. There is a need for one- and two-column footnotes.
4. Document the code.
5. Port the “place it here” code to three columns so it could be used for other formats.

6. A Comment on the Future of \TeX

\TeX must be enhanced with multiple-column formatting, object-placement options, and other related commands if it is to remain viable in the years ahead. WYSIWYG systems (such as Interleaf and Frame) that combine WYSIWYG with batch formatting in an effort to allow users to use tags for Standard Generalized Markup Language (SGML), will be tough competition for \TeX as it now stands. In addition to these features, math formatting will soon be offered by Frame.

With content tagging (SGML) soon to be a way of life for most of us as we enter the age of knowledge information processing, a good batch formatting system in the public domain would be of great value. We would like that system to be \TeX . We have a lot of \TeX experience to draw upon. However, the program can't perform the tasks its competitors are beginning to be able to address.

Some of the other enhancements we would like to see include:

1. An input file that could be buffered so that processing could be done on the contents of the buffer. A command such as `\inputbuffersize2000` would establish the size of the buffer in bytes.
2. The ability to do string searches on the contents of the buffer and process the buffer up to the point a string match was found. It would also be useful if string searches could be done on the contents of any box and the match point returned. Commands such as `\vsplit\mybox` to `\findstring{string arg}` would then be possible.
3. The ability to write the contents of the unprocessed buffer to another file.
4. The ability to write contents of any box or delineated string to an ASCII file.
5. The ability to create multiple `dvi` output files.
6. The ability to assign a variable as a real, as well as a dimension or count register. Full floating-point arithmetic would be available on these variables.